Published on 25 October 2019. Downloaded by Changchun Institute of Optics, Fine Mechanics and Physics, CAS on 6/16/2020 9:28:47 AM.

Nanoscale

PAPER

View Article Online
View Journal | View Issue

Check for updates

Cite this: *Nanoscale*, 2019, **11**, 21953

# Bone formation promoted by bone morphogenetic protein-2 plasmid-loaded porous silica nanoparticles with the involvement of autophagy†

Xiaowei Xu, *‡[a] Maolei Sun,‡[a] Dandan Wang,‡[a] Wenhuan Bu,[a] Zilin Wang,[a] Yuqin Shen,[a] Kai Zhang,[b] Ding Zhou,*[c] Bai Yang[b] and Hongchen Sun*[d]

Received 15th August 2019,
Accepted 23rd October 2019

DOI: 10.1039/c9nr07017f

rsc.li/nanoscale

Gene therapy is one of the most common and effective ways for the regeneration of defective bone tissue, but even highly efficient gene delivery vectors are insufficient. In this study, bone morphogenetic protein-2 plasmid (pBMP-2) was encapsulated by polyethylenimine-modified porous silica nanoparticles (PPSNs), which were synthesized *via* an ethyl ether emulsion method. Owing to the high specific surface area and high absorption characteristics, low cytotoxicity PPSNs can efficiently load and protect pBMP-2. The resulting PPSN/pBMP-2 can transfect MC3T3-E1 cells effectively to promote osteogenic differentiation and increase calcium deposition *in vitro*. Interestingly, the mass of calcium deposition nodules decreased dur to the presence of an autophagy inhibitor, demonstrating that PPSNs stimulated the autophagy pathway. Because of their excellent biocompatibility, high transfection efficiency, and ability to stimulate autophagy, the as-prepared PPSN/pBMP-2 could efficiently transfect local cells in a defect area *in vivo*. Micro-computed tomography and histological images demonstrated that PPSN/pBMP-2 could efficiently promote new bone formation in a 5 mm sized rat calvarial defect model. Taken together, our newly synthesized PPSNs could efficiently carry pBMP-2 and deliver it to the target cells as well as stimulating the autophagy pathway, resulting in significant osteogenic differentiation and bone regeneration.

## Introduction

Resorption defect of bone tissue is one of the most common clinical manifestations that could be induced by inflammation, trauma, tumor, aging and so forth. Seeking an effective way to prevent and inhibit bone resorption and promote bone formation is a fascinating issue for researchers in the field.[1] Bone grafting, tissue-engineering and distraction osteogenesis technology have been applied to treat resorption and defects of bone tissue and certain achievements have been gained after long term research and practice.[2–4] However, autologous bone or allograft can cause poor shaping, secondary injury as well as immunological rejection;[2] biomaterials and tissue-engineered artificial bone are limited in osteogenesis;[4] distraction osteogenesis technology is hard to popularize owing to its limited indications, complex operation technology and high price. Therefore, a novel or modified treatment for the resorption and defect of bone tissue is still in urgent need.

Decades in the making, gene therapy represents a major shift in medicine.[5] Many studies have demonstrated that gene therapy has been or will be unambiguously beneficial for many diseases.[6–10] The first gene therapy product, the first chimeric antigen receptor T-cell therapy Kymrich™, was approved by the United States Food and Drug Administration in 2017.[11] When applying gene therapy for the regeneration of a defective bone tissue, bone morphogenetic protein-2 plasmid (which we denote as pBMP-2 below, with a "p" standing for "plasmid") is critical, since its protein expression (*i.e.*, BMP-2) plays a key role in bone fracture healing, particularly in the early stage.[12–14] A previous study showed that BMP-2 is the earliest expression product after bone fracture occurs, can carry mesenchymal stem cells (MSCs) to the fracture sites to promote cartilage formation, and can play an important role in the initiation of cascade healing.[13,15,16] An *in vitro* study

[a]*School and Hospital of Stomatology, Jilin University, Changchun 130021, P. R. China. E-mail: xiaoweixu@jlu.edu.cn*
[b]*AState Key Laboratory of Supramolecular Structure and Materials, College of Chemistry, Jilin University, Changchun 130012, P. R. China*
[c]*State Key Laboratory of Luminescence and Applications, Changchun Institute of Optics, Fine Mechanics and Physics, Chinese Academy of Sciences, Changchun 130033, P. R. China. E-mail: zhouding@ciomp.ac.cn*
[d]*School and Hospital of Stomatology, China Medical University, Shenyang 110122, P. R. China. E-mail: sunhongchen@cmu.edu.cn*

†Electronic supplementary information (ESI) available: Zeta-potential of PSN-$NH_2$, PSN-COOH and PPSN, XPS spectra of C 1s in PSN-COOH and N 1s in PPSN, agarose gel electrophoresis retardation assay, and TEM images of MC3T3-E1 cells. See DOI: 10.1039/C9NR07017F

‡These authors contributed equally to this work.

Published on 25 October 2019. Downloaded by Changchun Institute of Optics, Fine Mechanics and Physics, CAS on 6/16/2020 9:28:47 AM.

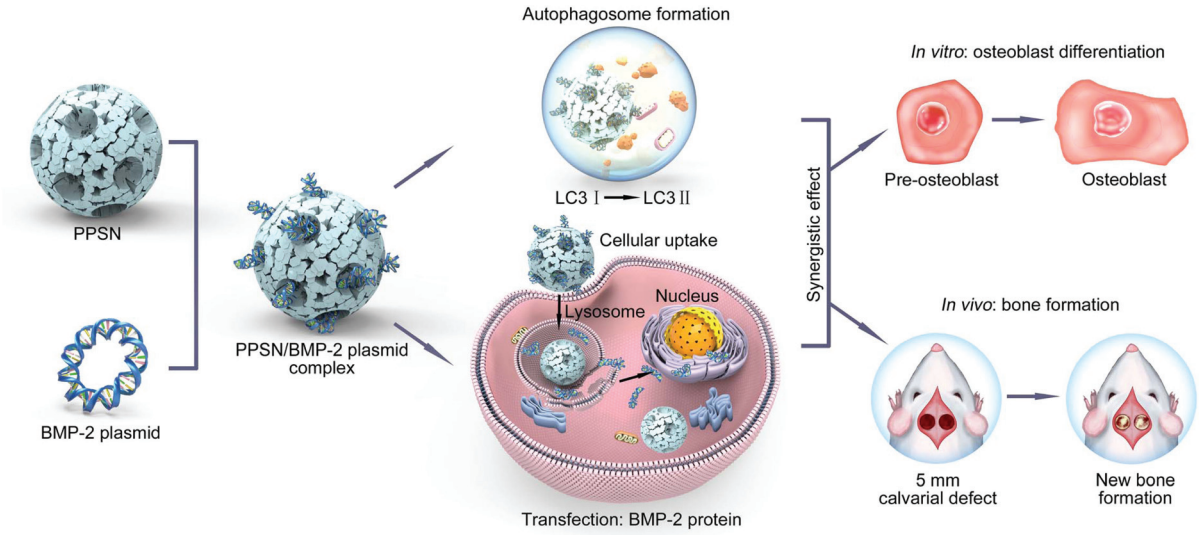


**Scheme 1** Schematic of the preparation and application of PPSN/pBMP-2.

showed that BMP-2 could be involved in bone metabolism *via* BMP/Smad signaling pathways and induce MSCs to differentiate into an osteoblast phenotype.[13] In addition to stimulating cell differentiation directly, BMP-2 promoted bone healing by inducing the expression of endogenous osteoinductive growth factors.[12] To promote bone formation, the continuous infusion of BMP-2 is necessary, since BMP-2 cannot be retained for a long time after application. Direct use of a recombinant protein is expensive and time-consuming.[17–20] Thus, pBMP-2 shows great potential for application in the stimulation of bone regeneration. Nevertheless, how to deliver pBMP-2 into cells and apply it without degradation are still major issues.

Vectors, which are used to carry therapeutic genes into the cells, are a major factor for a successful gene therapy treatment.[21–23] Although viral vectors are very useful and efficient in gene therapy, they always have strong toxicity and can cause immune responses.[24] These disadvantages continually prompt researchers to optimize current vectors or find adaptive non-viral vectors.[21,25–27] In general, non-viral vectors could cause less cytotoxicity and immune response, but also have less transfection efficiency than the viral ones.[26] Among non-viral vectors, nanomaterials become an interesting vector system with the merits of controllable surface-functionalization and no or few side effects.[28–30] In particular, when internalizing nanomaterials into cells, autophagy may be a possible cellular intermediate, which is favorable to bone formation, since autophagy plays an interesting role in bone homeostasis and mineralization balance in bone marrow mesenchymal stem cells, osteoblasts, osteoclasts and osteocytes.[31–33] Silica nanoparticles (SNs) are widely studied in biomedical research due to their good stability, biocompatibility, and low immunogenicity.[34] However, the application of SNs as a gene vector is limited due to their low transfection efficiency.[35] Thus, improving the transfection efficiency of SNs is critical for the development of nano gene therapy vectors.

In this study, to create an efficient pBMP-2 delivery system for effectively stimulating new bone formation, $NH_2$-decorated porous SNs (PSN-$NH_2$) with a high specific surface area were synthesized *via* an ethyl ether emulsion method. Through further successive modification by succinic anhydride and polyethylenimine (PEI), PEI-decorated PSNs (PPSNs) with positive charge were obtained, which could efficiently encapsulate pBMP-2 *via* strong electrostatic interactions. *In vitro* and *in vivo* experimental results indicated that the resultant pBMP-2-loaded PPSNs (PPSN/pBMP-2) presented excellent biocompatibility and high transfection efficiency, and therefore promote osteogenic differentiation and bone formation. Moreover, autophagy, which is stimulated by PPSNs, is demonstrated to participate in this process to enhance the osteogenic differentiation and new bone formation (Scheme 1).

## Results and discussion

### Characteristics of PPSNs

PSN-$NH_2$ were synthesized *via* an ethyl ether emulsion synthesis procedure, where tetraethyl orthosilicate and 3-aminopropyl triethoxysilane (KH550), ammonia, cetyltrimethylammonium bromide (CTAB), and ethyl ether were used as co-condensation silanes, catalyst, surfactant, and pore-forming agent, respectively (see Experimental section for details). During the gelation process of silica, ethyl ether volatilized slowly but ceaselessly, resulting in the formation of a pore structure. Under scanning electron microscope (SEM) observation, the PSN-$NH_2$ possessed a uniform particle size of 110–230 nm and numerous center-radial pores on the external surface (Fig. 1a and d). The zeta potential of PSN-$NH_2$ is measured to be 6.2 ± 0.6 mV (Table S1†), indicating the presence of amino groups in the PSN-$NH_2$.

These unique pore structures encouraged us to utilize PSN-$NH_2$ as a delivery vector for gene transfer. PSN modified

 This journal is © The Royal Society of Chemistry 2019

Published on 25 October 2019. Downloaded by Changchun Institute of Optics, Fine Mechanics and Physics, CAS on 6/16/2020 9:28:47 AM.

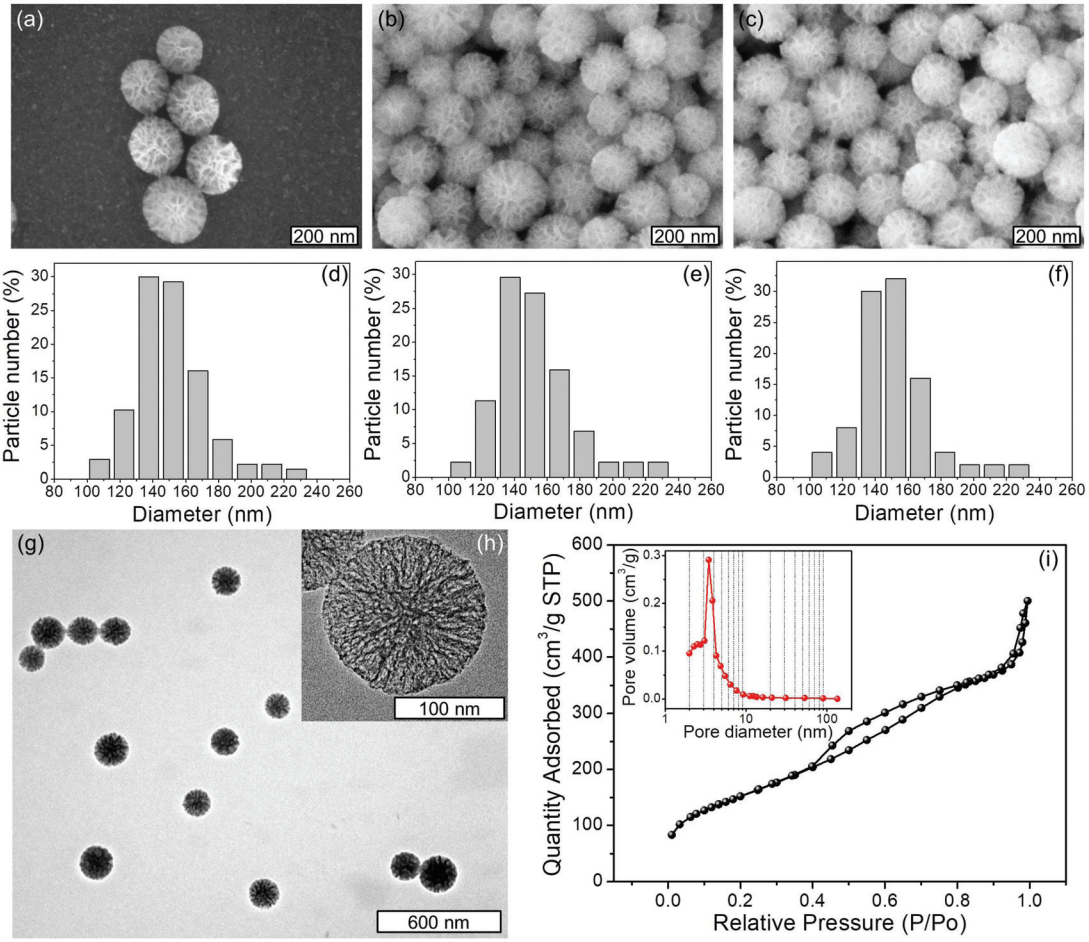


**Fig. 1** (a–c) SEM images and (d–f) the corresponding size distributions of (a and d) PSN-$NH_2$, (b and e) PSN-COOH, and (c and f) PPSNs. HRTEM images of PPSNs at low (g) and high (h) magnification. (i) Nitrogen sorption data of PPSNs.

with carboxyl groups (PSN-COOH) were fabricated by the reaction between the amino groups of PSN-$NH_2$ and succinic anhydride.

Fig. 1b and e indicate that there was no change in the particle size and size distribution compared to that in PSN-$NH_2$. The resultant PSN-COOH possesses a negative potential of −9.8 ± 0.5 mV due to presence of the carboxyl groups (Table S1†). The existence of the carboxyl groups was also confirmed by X-ray photoelectron spectroscopy (XPS) analysis of the C 1s spectrum. Fig. S1a† shows the C 1s spectrum of PSN-COOH, which is fitted to two separate peaks at 288.5 and 284.7 eV, respectively. The former is assigned to –COOH and the latter is assigned to $-CH_2-$. Furthermore, PPSNs were prepared by grafting branched PEI onto PSN-COOH *via* the amidation reaction between PEI and PSN-COOH. Similarly, PPSNs show no change in size and are still monodisperse, favorable for entering a cell for gene transfection (Fig. 1c and f). The pore structures of PPSNs are further confirmed by high resolution transmission electron microscopy (HRTEM) image (Fig. 1g), indicating that the average pore size is ~4.5 nm, as validated by nitrogen sorption data (Fig. 1i). XPS measurements confirm that amino groups belonging to PEI exist in PPSNs (Fig. S1b†), resulting in a high positive zeta potential of 50.3 ± 0.8 mV (Table S1†). Therefore, *via* strong electrostatic interactions, PPSNs are expected to efficiently encapsulate negatively charged pBMP-2 for gene transfer.

### Cytotoxicity of PPSNs

3-(4,5-Dimethyl-2-thiazolyl)-2,5-diphenyl-2-*H*-tetrazolium bromide (MTT) and apoptosis assays were used to evaluate the cytotoxicity of PPSNs. Fig. 2a shows that the cell proliferation rate slightly decreased at a relatively lower concentration (under 40 μg $mL^{-1}$ of PPSNs, $P > 0.05$) and significantly decreased at 80 μg $mL^{-1}$ of PPSNs ($P < 0.01$). It suggested that the effect of PPSNs on cell proliferation was dose-dependent. A cell apoptosis assay was used for the further analysis of cytotoxicity effects of PPSNs. Data from the apoptosis assay demonstrated that PPSNs could slightly increase the cell apoptosis rate in a dose-dependent manner (Fig. 2b–f).

### Transfection ability of PPSNs

To evaluate if PPSNs can be used as gene vectors, the frequently-used enhanced green fluorescent protein plasmid (pEGFP) was adopted to investigate the binding capacity of

Published on 25 October 2019. Downloaded by Changchun Institute of Optics, Fine Mechanics and Physics, CAS on 6/16/2020 9:28:47 AM.

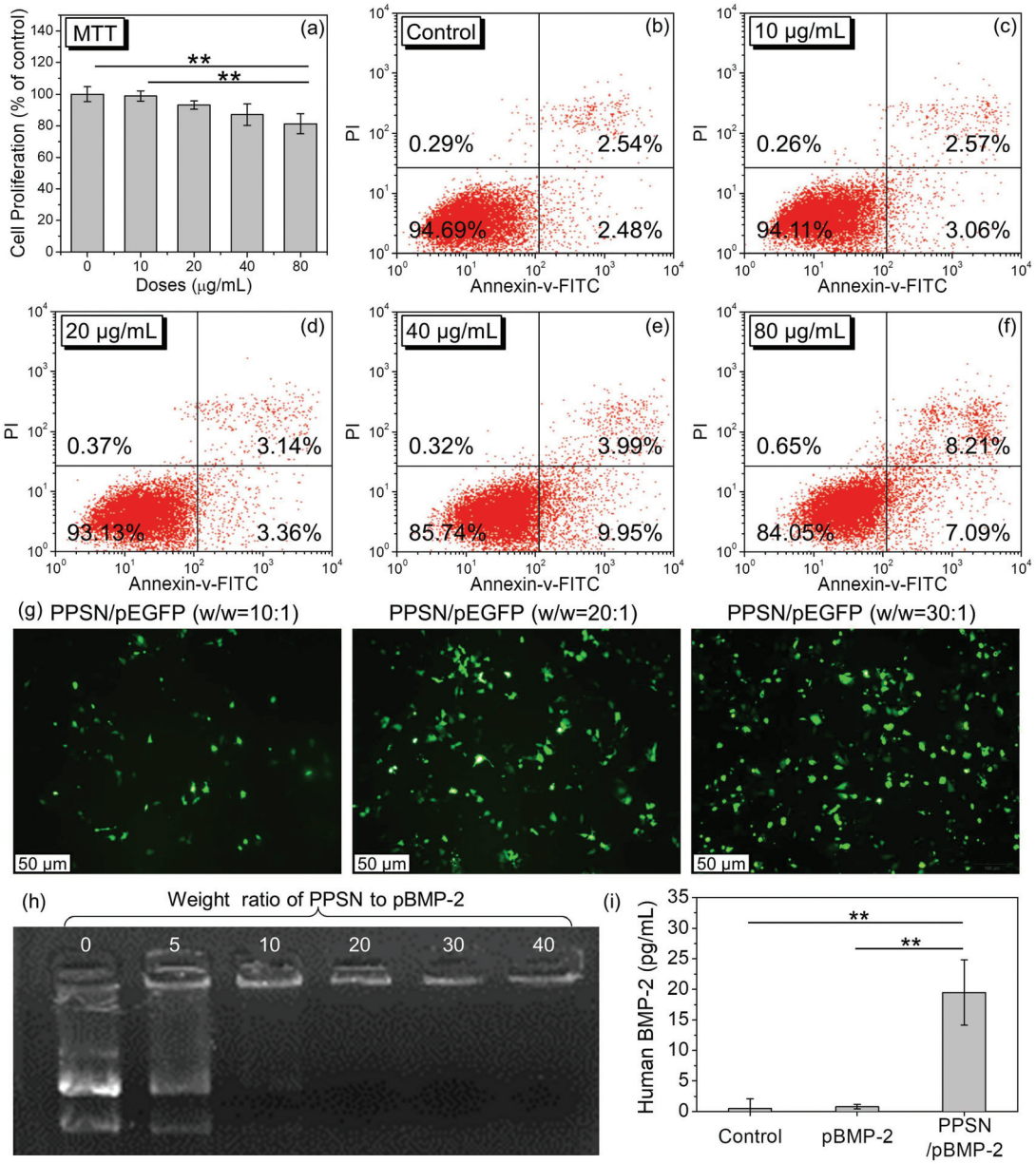


**Fig. 2** Cytotoxic effects of PPSN on MC3T3-E1 cells. (a) Data from the MTT assay. (b–f) FACS data from the apoptosis assay. (b) Control group. (c) PPSNs at 10 μg $mL^{-1}$. (d) PPSNs at 20 μg $mL^{-1}$. (e) PPSNs at 40 μg $mL^{-1}$. (f) PPSNs at 80 μg $mL^{-1}$. (g) Transfection efficiency by EGFP positive cells. 293 T cells were transfected with PPSNs and pEGFP at various weight ratios of 10 : 1, 20 : 1 and 30 : 1. (h) Agarose gel electrophoresis retardation assay. PPSNs and pBMP-2 at various weight ratios of 0 : 1, 5 : 1, 10 : 1, 20 : 1, 30 : 1 and 40 : 1. (i) Transfection efficiency by measuring BMP-2 secretion. Data are presented as mean ± SD from three experiments. *$P < 0.05$, **$P < 0.01$.

PPSNs. Agarose gel electrophoresis was performed at various PPSN: pEGFP weight ratios of 0 : 1, 5 : 1, 10 : 1, 20 : 1, 30 : 1 and 40 : 1 (Fig. S2†). Results showed a band migrated out from the well at the ratio 5 : 1 (Fig. S2†), indicating that pEGFP is not completely combined with PPSNs. When the ratio reached 10 or above, the migration of pEGFP was completely retarded (Fig. S2†). This suggested that the pEGFP was totally combined with PPSNs after the ratio of 10 : 1. Subsequently, the transfection efficiency of the pEGFP-loaded PPSNs was evaluated using 293 T cells. Data show that green fluorescent positive cells increased with the increase in PPSNs to pEGFP ratio after 48 h and the highest transfection efficiency (27.1%) is at the ratio of 30 : 1 (9.4% at ratio of 10 : 1 and 22.1% at ratio of 20 : 1) (Fig. 2g).

More importantly, PPSNs also exhibit strong binding capacity with pBMP-2 for the formation of PPSN/pBMP-2. The results of the agarose gel electrophoresis show that there is still a weak band migrating out from the well at ratio of 10 : 1, indicating an incomplete combination of PPSNs and pBMP-2 (Fig. 2h). PPSNs combined with pBMP-2 entirely when the ratio is higher than 10 : 1 (Fig. 2h), but when the ratio reaches 30 : 1, the concentration of PPSNs is about 80 μg $mL^{-1}$, leading

 This journal is © The Royal Society of Chemistry 2019

Published on 25 October 2019. Downloaded by Changchun Institute of Optics, Fine Mechanics and Physics, CAS on 6/16/2020 9:28:47 AM.

to obvious cytotoxicity (Fig. 2a–f). Therefore, the optimized weight ratio of PPSN/pBMP-2 is 20 : 1. Furthermore, as indicated by the enzyme-linked immunosorbent assay (ELISA), PPSN/pBMP-2 can effectively transfect 293 T cells and express human BMP-2, while nearly no human BMP-2 expression occurs in 293 T cells transfected with pBMP-2 alone (Fig. 2i).

In all, PPSNs exhibit strong binding capacity with plasmid and high transfection efficiency, which is mainly ascribed to the PEI-modified surface.[36,37] It is well known that the entrapment and degradation of plasmids in lysosome limit the delivery efficiency of the target gene into the nucleus; thus, delivering pBMP-2 alone could not lead to the human BMP-2 expression (Fig. 2i). Escape from lysosome is of significant importance for gene delivery. In PPSN/pBMP-2, there are abundant PEI, which can buffer the pH in the lysosomal compartments. PEI lead to a massive proton accumulation, followed by passive chloride influx, which cause lysosomal osmotic swelling and subsequent rupture of the lysosomal membranes, finally releasing plasmid into the cytoplasm.[38] Therefore, PPSN/pBMP-2 could be a promising candidate for the treatment of bone defect.

### *In vitro* mineralization assessment of PPSN/pBMP-2

To evaluate if PPSN/pBMP-2 could stimulate osteogenesis *in vitro*, alizarin red staining was employed to identify mineralization. Fig. 3a–c shows that positive red calcium deposition nodules could be seen in all three groups. The PPSN/pBMP-2 group, however, clearly had the highest positive result for red calcium deposition nodules (Fig. 3c). Interestingly, there are more positive red calcium deposition nodules in the PPSN group than those in the control group, which indicated that PPSNs alone could induce osteogenic differentiation to some degree.[39] Furthermore, the quantitative analysis also demonstrates that the PPSN/pBMP-2 group has the highest calcium deposition in all three groups (Fig. 3d). PPSNs alone can also promote osteogenic differentiation, which is supposed to be associated with autophagy, as mentioned in other reports.[40]

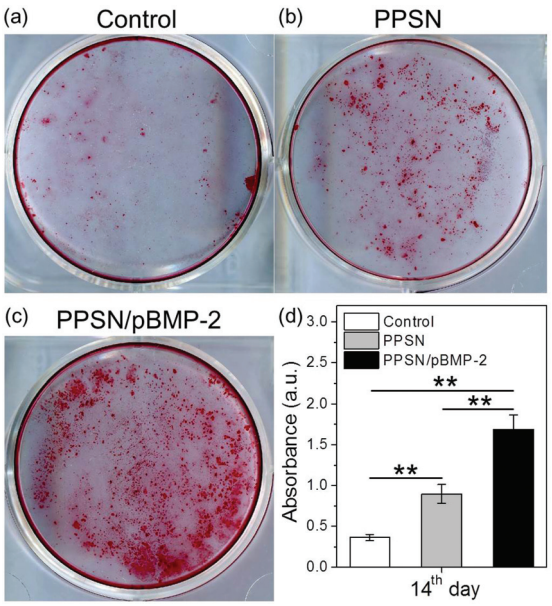


**Fig. 3** Effects of PPSN and PPSN/pBMP-2 on mineralization using MC3T3-E1 cells with alizarin red staining. (a) Control. (b) PPSNs at 50 μg $mL^{-1}$ and (c) PPSN/pBMP-2 at weight ratio of 20 : 1. (d) Bar graph of quantitative alizarin red staining by spectrophotometry at 562 nm. Data from all three experiments are presented as mean ± SD. *$P$ < 0.05, **$P$ < 0.01.

### Effects of autophagy on osteogenic process in PPSN/pBMP-2 treated cells

Autophagy flux increases significantly in the early stage of osteogenic differentiation and mineralization, suggesting that autophagy is closely related to osteogenic differentiation and mineralization.[41] To determine if autophagy is involved in the osteogenic process, we first detected autophagosome or autolysosome by morphological observation using TEM. Fig. 4a shows that there is significant increase in the number of mature autophagosomes or autolysosomes in PPSNs or PPSN/pBMP-2 treated groups at 24 h post-transfection, compared to that in the control group. These results suggested that both PPSN and PPSN/pBMP-2 could promote autophagy. Subsequently, the acridine orange (AO) staining assay was further applied to detect autophagosomes. AO is a pH sensitive dye to mark acid vesicle organelles in cells.[40] The change from green to red in the cytoplasm indicates the formation of autophagosomes. As shown in Fig. 4b, the images indicate that most MC3T3-E1 cells have red color in the cytoplasm at 24 h post-treatment with PPSN or PPSN/pBMP-2, while most MC3T3-E1 cells in the control group were just green, further demonstrating the stimulation of autophagy by PPSNs and PPSN/pBMP-2. The quantitative analysis for the AO staining assay indicates that the fluorescence intensity ratio of red to green is only 0.31 in the control group, whereas the ratios in both PPSNs and PPSN/pBMP-2 groups exhibit higher values (1.38 and 1.47, respectively) (Fig. S3†). It is worth mentioning that pBMP-2 alone could not stimulate autophagy, which is confirmed by TEM image and AO staining assay (Fig. S4†). The recombinant human bone morphogenetic protein 2 (rhBMP-2) protein only group was carried out for comparison (Fig. S5†). AO staining assays show that the fluorescence of most MC3T3-E1 cells in both control and rhBMP-2 protein only groups are nearly identical and only green. The corresponding quantitative analysis of AO staining assays is conducted through comparing the fluorescence intensity ratio of red to green in these two groups and the results suggest that the fluorescence intensity ratios are both at low levels (0.31 and 0.30, respectively) and show no significant difference between them, indicating the formation of few autophagosomes. These results indicate the stimulation of autophagy is realized by nanomaterials (*i.e.*, PPSN) and the observation of autophagy in PPSN/pBMP-2 is also mainly because of the existence of PPSNs.[42]

From previous studies,[43] it is widely believed that autophagy may be a common cellular response to nanomaterials, including silica nanoparticles, while the definite mechanisms

Published on 25 October 2019. Downloaded by Changchun Institute of Optics, Fine Mechanics and Physics, CAS on 6/16/2020 9:28:47 AM.

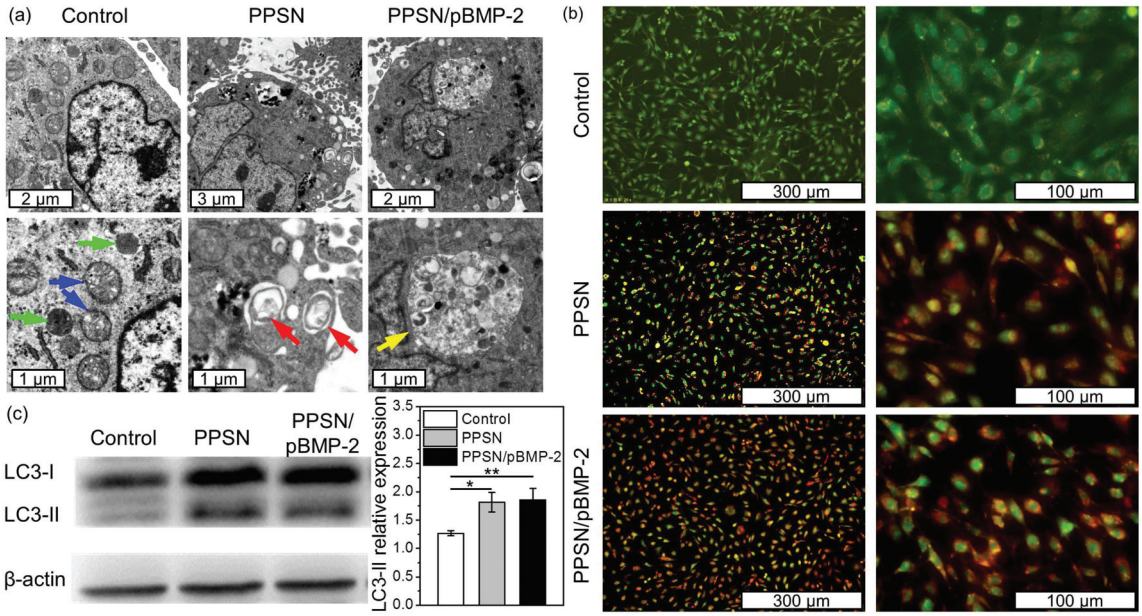


**Fig. 4** Association between autophagy and PPSNs or PPSN/pBMP-2 in MC3T3-E1 cells without treatment (control), MC3T3-E1 cells treated with PPSN at 50 μg per well and MC3T3-E1 cells treated with PPSN/pBMP-2 at the weight ratio of 20 : 1. (a) TEM images. Green arrows indicate lysosome, blue arrows indicate mitochondria, red arrows indicate autophagosomes, and yellow arrows indicate autolysosomes. The images of the upper row are taken at low magnification and the corresponding images taken at high magnification are shown in the lower row. (b) AO staining. The cells changed from green to red indicate the formation of autophagosomes. (c) Western blot data. Data from all three experiments are presented as mean ± SD. $*P < 0.05$, $**P < 0.01$.

responsible for nanomaterial-mediated autophagy induction are still not clearly delineated. At present, the autophagy activated by silica nanoparticles is generally attributed to oxidative stress.[44] After cellular uptake of PPSNs, PPSNs could accumulate in lysosomes and/or deposit in mitochondria,[45,46] which would disturb the electron transport chain and generate superoxide anion from molecular oxygen *via* one-electron reduction and further reductions, ultimately leading to mass production of reactive oxygen species.[46] After forming the autophagy microenvironment induced by PPSNs, autophagic vacuoles could be used as vehicles in osteoblasts to secrete apatite crystals[47] and the activation of ERK1/2 signaling pathway could lead to osteogenic differentiation.[42] Nanomaterials usually stimulate autophagosome assembly by the ERK1/2 signaling pathway, which is important for the conversion from LC3I to LC3II.[42] Thus, to further evaluate if PPSNs or PPSN/pBMP-2 is involved in autophagy, western blot was carried out to verify the formation of autophagosome structure (*i.e.*, conversion from LC3I to LC3II). Fig. 4c reveals that after 24 h treatment with PPSN or PPSN/pBMP-2, the densities of LC3-II protein bands are increased in both PPSNs (1.43 fold, $P < 0.05$) and PPSN/pBMP-2 (1.47 fold, $P < 0.01$) groups, which indicates that a stimulating effect on LC3II conversion occurred, with no obvious conversion in the control group.

To further understand the role autophagy and pBMP-2 expression play in osteogenesis, we evaluated osteogenic differentiation and mineralization after pretreatment with autophagy inhibitor 3-methyladenine (3-MA). After 24 h, only a few MC3T3-E1 cells have red color in their cytoplasm post-treatment with PPSN or PPSN/pBMP-2 compared with MC3T3-E1 cells in the control group, further demonstrating the inhibition of autophagy by addition of 3-MA (Fig. S6†). Fourteen days after application of 3-MA in the control, PPSN and PPSN/pBMP-2 groups, obvious calcium nodules were only observed in the PPSN/pBMP-2 group, mainly due to the pBMP-2 expression (Fig. 5d). However, there was nearly no formation of

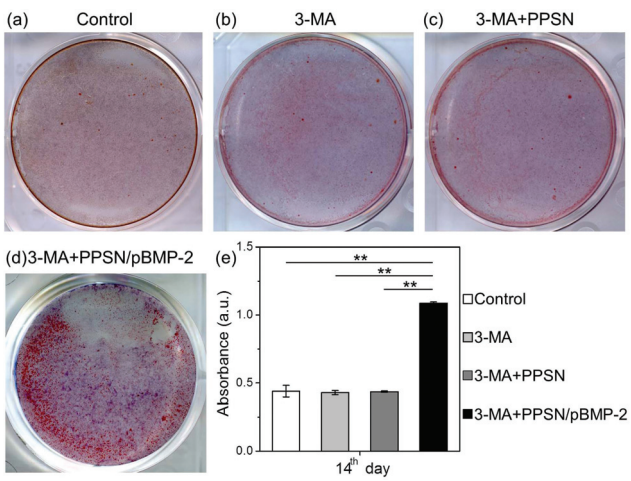


**Fig. 5** Effects of autophagy inhibitor (3-MA, 3 mM) on mineralization. (a) Control. (b) 3-MA. (c) 3-MA + PPSN. (d) 3-MA + PPSN/pBMP-2. (e) Bar graph of quantitative alizarin red staining by spectrophotometry at 562 nm. Data from all three experiments are presented as mean ± SD. $*P < 0.05$, $**P < 0.01$.


This journal is © The Royal Society of Chemistry 2019

Published on 25 October 2019. Downloaded by Changchun Institute of Optics, Fine Mechanics and Physics, CAS on 6/16/2020 9:28:47 AM.

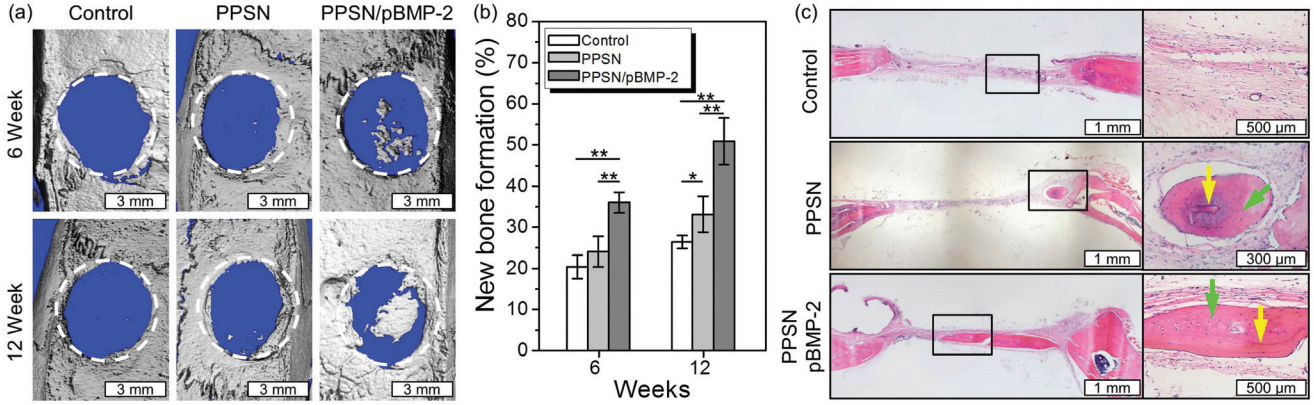


Fig. 6 Biological effects of PPSN or PPSN/pBMP-2 on new bone formation by micro-CT and H&E staining. Control group is rat calvarial bone defect without treatment; PPSN group is treated with 200 μg of PPSN; PPSN/pBMP-2 group is treated with PPSN/pBMP-2 at weight ratio of 20 : 1 at 6 and 12 weeks post-treatment. (a) Images of micro-CT. (b) Quantitative data from micro-CT. (c) H&E staining at 12 weeks post-treatment. Green arrows indicate osteoblasts and yellow arrows indicate reversal line. Data from all three experiments are presented as mean ± SD. $*P < 0.05$, $**P < 0.01$. Here, one way ANOVA is adopted, since the evaluation of statistical significance is performed independently at two points post-treatment (*i.e.*, 6 and 12 weeks).

calcium nodules in the PPSN group, which could be ascribed to the inhibition of autophagy (Fig. 3b and 5c). These results indicate that PPSN can stimulate autophagy, which plays an important role in enhancement of osteogenic differentiation and in formation of more and larger mineralized nodules.

### *In vivo* effects of PPSN/pBMP-2 on osteogenesis

A 5 mm sized rat calvarial defect model was established to investigate *in vivo* osteogenesis (see Experimental section for details).[48] Micro-computed tomography (micro-CT) data demonstrated that very limited bone was formed in the defect areas of control and PPSN groups, while small dispersed pieces of new bone were observed in the middle of the defect area of PPSN/pBMP-2 group after 6 weeks (Fig. 6a). The new bone formation area of PPSN/pBMP-2 group reached 36.1 ± 2.5%, which was 1.8-fold that of the control group (20.4 ± 2.8%) after 6 weeks (Fig. 6b). After 12 weeks, obvious osteogenesis occurred in the center and edge of the defect areas of PPSN/pBMP-2 group, while there was hardly any difference in bone mass at the end of the 6$^{th}$ week and 12$^{th}$ week in the control group and PPSN group (Fig. 6a and b). The new bone formation areas reached 50.9 ± 5.7% in PPSN/pBMP-2 group, 26.4 ± 1.6% in control group and 33.2 ± 4.4% in PPSN group (Fig. 6b). Further, the hematoxylin and eosin (H&E) staining results confirmed the micro-CT data. After 12 weeks, only a small amount of new bone tissue was observed on both ends of the defect areas in the control group, whereas obvious fibrous connective tissue was observed in the defect areas (Fig. 6c). In general, the results in PPSN group were nearly identical to the control group. This group had a little more osteoid tissue or new bone formation on both ends of the defect areas in the PPSN group compared to the control group (Fig. 6c). However, new bone formation was dramatically increased on both ends of the defect areas and in the center area in the PPSN/pBMP-2 group (Fig. 6c). Many osteocytes were observed in the new bone areas and single-layer flat osteoblasts were seen surrounding the new bone tissue, which indicate that osteogenesis occurred in these locations (Fig. 6c). Our data further confirm that pBMP-2 can be used as a bone regeneration agent to treat bone defect. All the above results demonstrate that an effective delivery system has been created to enhance and promote new bone formation *in vivo* through multiple effectors of PPSN, pBMP-2 and autophagy.

In order to further support the involvement of autophagy in PPSN-induced osteogenesis at the bone defect area, immunohistochemistry (IHC) staining is applied to detect the level of LC3, the biomarker of the formation of autophagosomes, by specifically binding with LC3 antibodies in the rat calvarial bone defect area (Fig. S7†). The quantities of LC3 positive cells in both PPSN and PPSN/pBMP-2 groups are obviously more than that in the control group. These results further confirmed that autophagy is involved in PPSN-induced osteogenesis at the bone defect area.

### *In vivo* biocompatibility assessment of PPSN/pBMP-2

In addition, the possible toxicity of PPSN/pBMP-2 was evaluated by using H&E staining on heart, liver, spleen and kidney, after *in vivo* application of PPSN/pBMP-2. There was no histological abnormity in heart, liver, spleen or kidney among control, PPSN and PPSN/pBMP-2 groups (Fig. S8†). These data suggest that the doses of PPSN and PPSN/pBMP-2 used here are safe for *in vivo* applications.

## Experimental section

### Synthesis of PPSN

An ethyl ether emulsion approach was used to prepare $NH_2$-decorated porous silica nanoparticles (PSN-$NH_2$).[49] In this one-pot sol–gel reaction system, cetyltrimethylammonium bromide (CTAB, ≥99% pure, Beijing Chemical Reagents Company,

Published on 25 October 2019. Downloaded by Changchun Institute of Optics, Fine Mechanics and Physics, CAS on 6/16/2020 9:28:47 AM.

Beijing, China) was used as a surfactant, ammonia as a catalyst, and tetraethyl orthosilicate (TEOS) and 3-aminopropyl triethoxysilane (KH550) as co-condensation silanes. Briefly, 0.5 g of CTAB was dissolved in 70 mL of deionized water, then 0.8 mL of aqueous ammonia, 15 mL of ethyl ether and 5 mL of ethanol were added under magnetic stirring at 1000 rpm for 0.5 h at room temperature. 2.5 mL of TEOS and 0.1 mL of KH550 were added dropwise to the reaction system and continuous stirring at 1000 rpm was applied for 6 h. Finally, 1 mL of HCl (37%) was added and the whole system was stirred for 10 min. The PSN-$NH_2$ were collected *via* centrifugation (8000 rpm, 15 min) and then alternately dispersed and centrifuged with ethanol and deionized water twice. Afterward, the PSN-$NH_2$ were dispersed in 120 mL of ethanol and then 15 mL of HCl (37%) was added into the PSN-$NH_2$, followed by stirring at 70 °C for 24 h in order to remove the CTAB template. The final product was obtained by centrifuging at 8000 rpm for 10 min, washing with water and ethanol twice alternately, and then freeze-drying for use.

Fifty mg of PSN-$NH_2$ were dispersed in 20 mL of *N*,*N*-dimethylformamide (DMF), then 0.45 g of succinic anhydride was dissolved in 5 mL of DMF and added into the suspension. Subsequently, 0.45 mL of triethanolamine (TEA) was added and the mixture was stirred at 600 rpm for 6 h at room temperature. In order to obtain the carboxyl groups-modified PSN (PSN-COOH), the product was centrifugated at 8000 rpm for 10 min, washed with water and ethanol twice each to remove TEA and excessive succinic anhydride, then freeze-dried for use.

Twenty mL of DMF containing 30 mg of PSN-COOH, 32 mg of 1-ethyl-3-(3-dimethylaminopropyl) carbodiimide hydrochloride (EDC) and 19 mg of *N*-hydroxysuccinimide (NHS) was mixed and stirred at 600 rpm for 30 min at room temperature. 0.2 mL of polyethylenimine (PEI, 100 mg $mL^{-1}$) and 1 mL of ethanol were added dropwise to the reaction system and stirred continually at 600 rpm for 5 h at room temperature. In order to obtain the PEI-modified PSN (PPSN), the product was centrifugated at 8000 rpm for 10 min, washed with water and ethanol twice alternately to remove EDC, NHS and excessive PEI, and then freeze-dried for use.

### Characteristics of PPSN

Morphology of the PPSN was examined with a scanning electron microscope (SEM) (FESEM6700F, JEOL, Tokyo, Japan). The zeta potential of PPSN was obtained using dynamic light scattering (DLS) (Zetasizer NanoZS, Malvern Instruments, Britain) at 25 °C. Transmission electron microscopy (TEM) was conducted in a Hitachi H-800 electron microscope at an acceleration voltage of 200 kV with a CCD camera. High-resolution TEM (HRTEM) imaging was implemented by a JEM-2100F electron microscope at 200 kV. X-ray photoelectron spectroscopy (XPS) was investigated using a VG ESCALAB MKII spectrometer with Mg KR excitation (1253.6 eV).

### Cell cultures

MC3T3-E1 (subclone-4), a mouse pre-osteoblast cell line, and 293 T, a human embryonic kidney cell line, were acquired from the Chinese Academy of Sciences Cell Bank (Shanghai, China) and cultured in Dulbecco's Modified Eagle Medium (DMEM) with high glucose, containing 10% fetal bovine serum (FBS) (Thermo Fisher Scientific, Grand Island, NY, USA), 100 U $mL^{-1}$ penicillin (Thermo Fisher Scientific) and 100 mg $mL^{-1}$ streptomycin (Thermo Fisher Scientific). Cells were incubated at 37 °C in humidified 5% $CO_2$ and the medium was changed every 2–3 days.

### Cytotoxicity assays of PPSN

3-(4,5-Dimethyl-2-thiazolyl)-2,5-diphenyl-2-*H*-tetrazolium bromide (MTT) assay was used to assess the cytotoxicity of PPSN *in vitro*. MC3T3-E1 cells were seeded in 96-well plates at $8 \times 10^4$ cells per well and cultured for 24 h. The medium was replaced with 200 μL medium containing 0, 10, 20, 40 or 80 μg $mL^{-1}$ of PPSN and continually cultured. After 24 h, 20 μL of MTT (5 mg $mL^{-1}$) was added to each well and incubated for 4 h until purple precipitate was formed. Then, the medium was removed and 150 μL of dimethyl sulfoxide was added into each well. Absorbance was measured at 570 nm using a microplate reader (RT-6000; Lei Du Life Science and Technology Co, Shenzhen, China). The cell viability was presented as a percentage of the control group, which was considered 100%.

Cell apoptosis assay was utilized to further clarify if the synthesized PPSN induces cytotoxicity. MC3T3-E1 cells were seeded in a 6-well plate at $2 \times 10^5$ cells per well and cultured for 24 h. The medium was replaced with 2 mL medium containing 0, 10, 20, 40 or 80 μg $mL^{-1}$ of PPSN and continually cultured for 24 h. The control group was treated without PPSN. Cells were harvested by trypsinization and washed twice with chilled phosphate buffer solution (PBS). Subsequently, they were resuspended in binding buffer and stained by Annexin V-FITC/PI apoptosis assay kit (Thermo Fisher Scientific) according to the manufacturer's instructions. Stained cells were analyzed by fluorescence-activated cell sorting (FACS, Becton Dickinson Biosciences, Drive Franklin Lakes, America).

### Agarose gel electrophoresis assay

Agarose gel electrophoresis was used to examine the mixture of plasmid with PPSNs. PPSNs and enhanced green fluorescent protein plasmid (pEGFP) or bone morphogenetic protein-2 plasmid (pBMP-2) were mixed at various weight ratios of 0 : 1, 5 : 1, 10 : 1, 20 : 1, 30 : 1 and 40 : 1, and then incubated at room temperature for 30 min. Ten μL of mixture was mixed with 2 μL of loading buffer, loaded into 1.0% agarose gel, electrophoresed at 100 V for 30 min, and then imaged using a UVP Bioimaging System (BIO-RAD, California, USA).

### Transfection efficiency assay

The 293 T cell line, a golden standard cell line for transfection efficiency, was used to evaluate the transfection efficiency of PPSN. 293 T cells were seeded in a 6-well plate at $2.5 \times 10^5$ cells per well, and cultured for 24 h. Then, the medium was replaced with serum-free medium. PPSN and pEGFP at weight ratios of 10 : 1, 20 : 1 and 30 : 1 were mixed and incubated at room temperature for 30 min. Afterward, the mixtures were

 This journal is © The Royal Society of Chemistry 2019

Published on 25 October 2019. Downloaded by Changchun Institute of Optics, Fine Mechanics and Physics, CAS on 6/16/2020 9:28:47 AM.

added into corresponding wells and cultured for 4 h, then the medium was replaced with DMEM and cultured for another 48 h. The transfected cells were observed by fluorescent inverted microscope (Olympus, Japan).

### Enzyme-linked immunosorbent assay (ELISA) to check human BMP-2 expression

Three groups, control, pBMP-2 and PPSN/pBMP-2 group were set up in this experiment. MC3T3-E1 cells were seeded in a 6-well plate at $2 \times 10^5$ cells per well and cultured for 24 h. The medium was replaced with serum-free medium for transfection. PPSN were mixed with pBMP-2 at a weight ratio of 20 : 1 for 30 min at room temperature, then the mixture was added into wells and cultured for 4 h. The control group was treated without PPSN or pBMP-2. After that, we replaced medium with DMEM for further culture. The supernatant was collected on day 3 for ELISA. Expression of pBMP-2 was determined by human BMP-2 ELISA kit (Boster Biological Technology, California, USA).

### Alizarin red staining assay

Alizarin red staining was used to evaluate mineralization ability of PPSN/pBMP-2. The control group was treated without PPSN or pBMP-2. MC3T3-E1 cells transfected with PPSN or PPSN/pBMP-2 were stained and analyzed at 14 days post-transfection, as reported in a previously published paper.[50] To further evaluate the role of autophagy in the mineralization ability, autophagy inhibitor 3-MA (3 mM, Sigma-Aldrich, St Louis, MO, USA) was added. After 14 days, the same staining procedure was used.

### Autophagy assays

To evaluate if autophagy is involved in the osteoblast differentiation, three assays were performed. The first was to observe MC3T3-E1 cells transfected with or without PPSN/pBMP-2 using a transmission electron microscope (TEM), which is a golden standard assay for autophagy. The control group was treated without PPSN or pBMP-2. MC3T3-E1 cells transfected with or without PPSN/pBMP-2 were harvested, fixed in 4% glutaraldehyde for 4 h, and then dehydrated with graded ethanol and embedded in epon (Sigma-Aldrich, St Louis, MO, USA). Ultrathin sections were stained with citrate and uranyl acetate and observed using TEM (TECNAI SPIRIT, FEI Company, Czech Republic).

Next is acridine orange (AO) staining. MC3T3-E1 cells transfected with or without PPSN/pBMP-2 were cultured for 24 h, washed twice with PBS and stained with 1 mg $mL^{-1}$ of AO for 1 min. Then, the stained cells were observed using a fluorescent inverted microscope (Olympus, Japan). To further evaluate the role of autophagy, 3-MA was added and the same staining procedure was used.

The final assay was western blot. MC3T3-E1 cells transfected with or without PPSN/pBMP-2 were cultured for 24 h. Then, cells were lysed using a radio immunoprecipitation assay buffer to extract cellular protein and the proteins were quantified by a BCA kit (Boster Biological Technology, California, USA). Twenty-five μg of protein from each sample was used to run 12% sodium dodecyl sulfate polyacrylamide gel electrophoresis (SDS-PAGE), then was transferred to a PDVF membrane. The blot was blocked with 5% non-fat milk of tris-buffered saline tween (TBST) (1× TBS plus 0.1% Tween 20) for 1 h and incubated with LC 3 primary antibody (1 : 500) (Abcam, no. 51520) overnight at room temperature. Afterward, the mixture was washed with TBST three times. A secondary antibody (1 : 5000) (Proteintech, SA00001-1) was added and incubated for 1 h at room temperature. Then, image data were obtained using a scanner (V750 PRO, EPSON, Indonesia) and band density was analyzed using the Image J software.

### *In vivo* osteogenic analysis by micro-computed tomography (Micro-CT) and histology assays

All animal procedures were performed in accordance with the Guidelines for Care and Use of Laboratory Animals of Jilin University and approved by the Animal Ethics Committee of Jilin University. Twenty-seven male Wistar rats (180–220 g) were randomly divided into three groups, control, PPSN and PPSN/pBMP-2 (at weight ratio of 20 : 1) ($n$ = 9). The surgical area of rats was shaved and sterilized after rats were anesthetized by 10% chloral hydrate (20 mg $kg^{-1}$). A 15–20 mm longitudinal incision was created behind the ear edge of rats, then the periosteum was bluntly separated. A 5 mm diameter circular defect area on the sagittal suture of the right-side skull was made using a hollow trephine bur and the bone was removed. During the process, the wound area was continuously flushed by normal saline for cooling and cleaning.

Two hundred μg of PPSN and 10 μg of pBMP-2 in 50 μL of PBS were mixed under magnetic stirring for 30 min. Fifty μL of PPSN or PPSN/pBMP-2 mixture was added dropwise to a gelatin sponge. Then, the gelatin sponge was implanted in the defect site and the incision was sutured with 3–0 nylon suture. Gelatin sponge with 50 μL of PBS was the control group.

Six or 12 weeks post-implantation, rats were anesthetized and euthanized by heart perfusion with 4% paraformaldehyde. Skull specimens were collected and fixed in 4% paraformaldehyde for 2 days, then analyzed by Micro-CT (μCT35, Scanco Medical AG, Bassersdorf, Switzerland) in a 20 mm diameter tube under fixed conditions (20 μm, 114 mA, 70 kVp and exposure time 300 ms). Then, all samples were decalcified in 10% ethylene diamine tetraacetic acid (EDTA) for two months. The EDTA solution was changed every week. Finally, samples were dehydrated in a graded series of ethanol, embedded in paraffin, sectioned at 5.0 mm, and stained with hematoxylin and eosin (H&E) staining. The sections were observed under a microscope.

### *In vivo* toxicity evaluation

Heart, liver, spleen and kidney were harvested from the abovementioned rats, fixed in 4% paraformaldehyde for 24 h, dehydrated in a graded series of ethanol, embedded in paraffin, sectioned at 5.0 mm, and stained with H&E staining.

### Statistical analysis

All experiments were repeated three times, except *in vivo* experiments. All values were presented as mean ± standard

Published on 25 October 2019. Downloaded by Changchun Institute of Optics, Fine Mechanics and Physics, CAS on 6/16/2020 9:28:47 AM.

deviation (SD). The results of the tests indicated that the $P$ values are greater than 0.05, demonstrating that the variance within each of the population is equal (*i.e.*, the homogeneity of variance is violated). Then, one-way ANOVA with Bonferroni *post hoc* tests was performed for the evaluation of statistical significances among the groups. $P < 0.05$ was considered to be statistically significant.

## Conclusions

In summary, we fabricated PPSNs with a positively charged surface *via* an ethyl ether emulsion approach and surface modifications, which effectively combined with negatively charged pBMP-2 *via* strong electrostatic interactions. The resulting PPSN/pBMP-2 exhibited excellent biocompatibility and can significantly promote osteogenic differentiation and new bone formation *in vitro* and *in vivo*. Meaningfully, autophagy, which could enhance osteogenic differentiation and new bone formation, is demonstrated to be stimulated by PPSNs. This study demonstrates PPSN/pBMP-2 have high transfection efficiency and can stimulate autophagy and further highlights the applicability of PPSN/pBMP-2 in bone defect treatments.

## Conflicts of interest

There are no conflicts to declare.

## Acknowledgements

This work was supported by grants from the National Key Research and Development Program of China 2016YFC1102800, the Natural Science Foundation of China (81970946, 81600879 and 81600890), Young Elite Scientist Sponsorship Program by CAST (2018QNRC001), China Postdoctoral Science Foundation (2018T110259 and 2016M601386), Jilin Province Education Department Science and Technology Research (JJKH20190106KJ), Jilin Province Science and Technology Research (20190103088JH), and JLU Science and Technology Innovative Research Team (2017TD-11).

## Notes and references

1 K. Park, *J. Controlled Release*, 2017, **254**, 137.
2 J. J. Li, M. Ebied, J. Xu and H. Zreiqat, *Adv. Healthcare Mater.*, 2018, **7**, 1701061.
3 S. I. Roohani-Esfahani and H. Zreiqat, *Nanomedicine*, 2017, **12**, 419.
4 F. M. Chen and X. H. Liu, *Prog. Polym. Sci.*, 2016, **53**, 86.
5 K. F. Buckland and H. Bobby Gaspar, *Adv. Drug Delivery Rev.*, 2014, **73**, 162.
6 M. H. Hassan, E. E. Othman, D. Hornung and A. Al-Hendy, *Adv. Drug Delivery Rev.*, 2009, **61**, 822.
7 R. E. MacLaren, M. Groppe, A. R. Barnard, C. L. Cottriall, T. Tolmachova, L. Seymour, K. R. Clark, M. J. During, F. P. M. Cremers, G. C. M. Black, A. J. Lotery, S. M. Downes, A. R. Webster and M. C. Seabra, *Lancet*, 2014, **383**, 1129.
8 F. Alderuccio, J. Chan, D. W. Scott and B. H. Toh, *Trends Mol. Med.*, 2009, **15**, 344.
9 C. Booth, H. B. Gaspar and A. J. Thrasher, *Trends Mol. Med.*, 2016, **22**, 317.
10 D. M. O'Connor and N. M. Boulis, *Trends Mol. Med.*, 2015, **21**, 504.
11 H. R. Mirzaei, A. Rodriguez, J. Shepphird, C. E. Brown and B. Badie, *Front. Immunol.*, 2017, **8**, 1850.
12 J. A. Cottrell, O. Keane, S. S. Lin and J. P. O'Connor, *J. Appl. Biomed.*, 2014, **12**, 127.
13 A. Oryan, S. Alidadi, A. Moshiri and A. Bigham-Sadegh, *BioFactors*, 2014, **40**, 459.
14 R. Garimella, S. E. Tague, J. H. Zhang, F. Belibi, N. Nahar, B. H. Sun, K. Insogna, J. X. Wang and H. C. Anderson, *J. Histochem. Cytochem.*, 2008, **56**, 569.
15 K. Tsuji, A. Bandyopadhyay, B. D. Harfe, K. Cox, S. Kakar, L. Gerstenfeld, T. Einhorn, C. J. Tabin and V. Rosen, *Nat. Genet.*, 2006, **38**, 1424.
16 S. Scarfi, *World J. Stem Cells*, 2016, **8**, 1.
17 R. J. O'Keefe and J. Mao, *Tissue Eng., Part B*, 2011, **17**, 389.
18 A. Sharma, F. Meyer, M. Hyvonen, S. M. Best, R. E. Cameron and N. Rushton, *Bone Joint Res.*, 2012, **1**, 145.
19 D. Sheyn, N. Kimelman-Bleich, G. Pelled, Y. Zilberman, D. Gazit and Z. Gazit, *Gene Ther.*, 2008, **15**, 257.
20 V. M. Betz, O. B. Betz, M. B. Harris, M. S. Vrahas and C. H. Evans, *Front. Biosci.*, 2008, **13**, 833.
21 I. Roy, T. Y. Ohulchanskyy, D. J. Bharali, H. E. Pudavar, R. A. Mistretta, N. Kaur and P. N. Prasad, *Proc. Natl. Acad. Sci. U. S. A.*, 2005, **102**, 279.
22 C. Dou, N. Ding, F. Luo, T. Y. Hou, Z. Cao, Y. Bai, C. Liu, J. Z. Xu and S. W. Dong, *Adv. Sci.*, 2018, **5**, 1700578.
23 K. Metavarayuth, P. Sitasuwan, J. A. Luckanagul, S. Feng and Q. Wang, *Adv. Sci.*, 2015, **2**, 1500026.
24 A. El-Aneed, *J. Controlled Release*, 2004, **94**, 1.
25 H. Y. Wang, Y. F. Jiang, H. G. Peng, Y. Z. Chen, P. Z. Zhu and Y. Z. Huang, *Adv. Drug Delivery Rev.*, 2015, **81**, 142.
26 M. Ramamoorth and A. Narvekar, *J. Clin. Diagn. Res.*, 2015, **9**, GE01.
27 H. Yin, R. L. Kanasty, A. A. Eltoukhy, A. J. Vegas, J. R. Dorkin and D. G. Anderson, *Nat. Rev. Genet.*, 2014, **15**, 541.
28 B. Pelaz, P. del Pino, P. Maffre, R. Hartmann, M. Gallego, S. Rivera-Fernandez, J. M. de la Fuente, G. U. Nienhaus and W. J. Parak, *ACS Nano*, 2015, **9**, 6996.
29 B. B. Manshian, D. F. Moyano, N. Corthout, S. Munck, U. Himmelreich, V. M. Rotello and S. J. Soenen, *Biomaterials*, 2014, **35**, 9941.
30 S. J. Soenen, W. J. Parak, J. Rejman and B. Manshian, *Chem. Rev.*, 2015, **115**, 2109.
31 L. J. Hocking, C. Whitehouse and M. H. Helfrich, *J. Bone Miner. Res.*, 2012, **27**, 1439.

 This journal is © The Royal Society of Chemistry 2019

Published on 25 October 2019. Downloaded by Changchun Institute of Optics, Fine Mechanics and Physics, CAS on 6/16/2020 9:28:47 AM.

32 M. R. Kaluderović, M. Mojić, J. P. Schreckenbach, D. Maksimović-Ivanić, H. L. Graf and S. Mijatović, *Cells Tissues Organs*, 2014, **200**, 265.
33 D. J. Klionsky, P. Codogno, A. M. Cuervo, V. Deretic, Z. Elazar, J. Fueyo-Margareto, D. A. Gewirtz, G. Kroemer, B. Levine, N. Mizushima, D. C. Rubinsztein, M. Thumm and S. A. Tooze, *Autophagy*, 2014, **6**, 438.
34 I. I. Slowing, J. L. Vivero-Escoto, C. W. Wu and V. S. Y. Lin, *Adv. Drug Delivery Rev.*, 2008, **60**, 1278.
35 D. R. Radu, C. Y. Lai, K. Jeftinija, E. W. Rowe, S. Jeftinija and V. S. Lin, *J. Am. Chem. Soc.*, 2004, **126**, 13216.
36 J. Q. Gao, Q. Q. Zhao, T. F. Lv, W. P. Shuai, J. Zhou, G. P. Tang, W. Q. Liang, Y. Tabata and Y. L. Hu, *Int. J. Pharm.*, 2010, **387**, 286.
37 H. Jin, K. Zhang, C. Y. Qiao, A. L. Yuan, D. W. Li, L. Zhao, C. Shi, X. W. Xu, S. L. Ni, C. Y. Zheng, X. H. Liu, B. Yang and H. C. Sun, *Int. J. Nanomed.*, 2014, **9**, 2179.
38 P. Neuberg and A. Kichler, *Adv. Genet.*, 2014, **88**, 263.
39 G. R. Beck Jr., S. W. Ha, C. E. Camalier, M. Yamaguchi, Y. Li, J. K. Lee and M. N. Weitzmann, *Nanomedicine*, 2012, **8**, 793.
40 Y. Wang, Y. X. Lin, Z. Y. Qiao, H. W. An, S. L. Qiao, L. Wang, R. P. Y. J. Rajapaksha and H. Wang, *Adv. Mater.*, 2015, **27**, 2627.
41 F. Liu, F. Fang, H. B. Yuan, D. Y. Yang, Y. Q. Chen, L. Williams, S. A. Goldstein, P. H. Krebsbach and J. L. Guan, *J. Bone Miner. Res.*, 2013, **28**, 2414.
42 S. W. Ha, M. N. Weitzmann and G. R. Beck Jr., *ACS Nano*, 2014, **8**, 5898.
43 S. T. Stern, B. S. Zolnik, C. B. McLeland, J. Clogston, J. W. Zheng and S. E. McNeil, *Toxicol. Sci.*, 2008, **106**, 140.
44 Y. B. Yu, J. C. Duan, Y. Yu, Y. Li, X. M. Liu, X. Q. Zhou, K. F. Ho, L. W. Tian and Z. W. Sun, *J. Hazard. Mater.*, 2014, **270**, 176.
45 J. Wang, Y. B. Yu, K. Lu, M. Yang, Y. Li, X. Q. Zhou and Z. W. Sun, *Int. J. Nanomed.*, 2017, **12**, 809.
46 S. N. Petrache Voicu, D. Dinu, C. Sima, A. Hermenean, A. Ardelean, E. Codrici, M. S. Stan, O. Zărnescu and A. Dinischiotu, *Int. J. Mol. Sci.*, 2015, **16**, 29398.
47 M. Nollet, S. Santucci-Darmanin, V. Breuil, R. Al-Sahlanee, C. Cros, M. Topi, D. Momier, M. Samson, S. Pagnotta, L. Cailleteau, S. Battaglia, D. Farlay, R. Dacquin, N. Barois, P. Jurdic, G. Boivin, D. Heymann, F. Lafont, S. S. Lu, D. W. Dempster, G. F. Carle and V. Pierrefite-Carle, *Autophagy*, 2014, **10**, 1965.
48 S. C. Zhao, J. H. Zhang, M. Zhu, Y. D. Zhang, Z. T. Liu, C. L. Tao, Y. F. Zhu and C. Q. Zhang, *Acta Biomater.*, 2015, **12**, 270.
49 X. Du, B. Y. Shi, J. Liang, J. X. Bi, S. Dai and S. Z. Qiao, *Adv. Mater.*, 2013, **25**, 5981.
50 X. K. Fu, Y. Y. Li, T. L. Huang, Z. W. Yu, K. Ma, M. Yang, Q. L. Liu, H. B. Pan, H. Y. Wang, J. F. Wang and M. Guan, *Adv. Sci.*, 2018, **5**, 1700755.